

Optimization of an inclined elliptic impinging jet with cross flow for enhancing heat transfer

Man-Woong Heo · Ki-Don Lee · Kwang-Yong Kim

Received: 25 May 2010/Accepted: 17 January 2011/Published online: 30 January 2011
© Springer-Verlag 2011

Abstract This work presents a parametric study and optimization of a single impinging jet with cross flow to enhance heat transfer with two design variables. The fluid flow and heat transfer have been analyzed using three-dimensional compressible Reynolds-averaged Navier-Stokes equations with a uniform heat flux condition being applied to the impingement plate. The aspect ratio of the elliptic jet hole and the angle of inclination of the jet nozzle are chosen as the two design variables, and the area-averaged Nusselt number on a limited target plate is set as the objective function. The effects of the design variables on the heat transfer performance have been evaluated, and the objective function has been found to be more sensitive to the angle of inclination of the jet nozzle than to the aspect ratio of the elliptic jet hole. The optimization has been performed by using the radial basis neural network model. Through the optimization, the area-averaged Nusselt number increased by 7.89% compared to that under the reference geometry.

List of symbols

A	Length along the parallel axis of the elliptic hole with respect to the cross flow direction
AR	Aspect ratio of the elliptic jet hole
B	Length along the perpendicular axis of the elliptic hole with respect to the cross flow direction
M	Blowing ratio (mass flux of jet flow/mass flux of cross flow)
D	Diameter of the jet nozzle

h	Heat transfer coefficient
h_0	Local heat transfer coefficient without jet flow
q	Heat flux on the wall
T_w	Bottom wall temperature
T_r	Ambient fluid temperature (reference temperature)
T_j	Inlet temperature of the jet flow (298[K])
Nu	Nusselt number
ρ	Density
U	Velocity
x	Downstream coordinate measured from the centre of the jet exit
z	Lateral coordinate measured from the centerline of the test section
θ	Angle of inclination of the jet nozzle
y+	Height of the first grid
ω_z	z-direction vorticity ($= \frac{1}{2} \left[\frac{\partial u}{\partial y} - \frac{\partial v}{\partial x} \right]$)
Φ	Dimensionless temperature ($= \frac{T_w}{T_j}$)

Subscripts/superscripts

j	Jet
∞	Main stream
-	Area-averaged quantity
*	Normalized value
stream	Streamwise direction
span	Spanwise direction
T.P.	Target plate

1 Introduction

Generally, an increase in the temperature of the working fluid is required for enhancing the thermal efficiency and specific thrust of gas turbines. However, due to the high temperature of the working fluid, a high thermal stress is

M.-W. Heo · K.-D. Lee · K.-Y. Kim (✉)
Department of Mechanical Engineering, Inha University,
253 Yonghyun-Dong, Nam-Gu,
Incheon 402-751, Republic of Korea
e-mail: kykim@inha.ac.kr

caused on the blade surface, which shortens the working life of the blades. Therefore, it is necessary to prevent the generation of a high thermal distribution on the blade surfaces.

Jet impingement cooling is one of the most effective cooling methods for hot objects by producing very large forced convective heat transfer rates. For this reason, jet impingement cooling has been widely used in many heat transfer applications including the internal cooling systems of turbine blades in gas turbine engines. Over several decades, several experimental and numerical investigations have been performed on jet impingement cooling to predict the fluid flow and heat transfer characteristics. For predicting the heat transfer characteristics of a jet impingement system, Bouchez and Goldstein [1] empirically investigated the effect of the spacing between the jet exit and the plate on the heat transfer coefficient for confined circular air jets that vertically impinged upon a flat plate under a specified uniform heat flux condition, and concluded that the ratio of heat transfer coefficient with jet flow to that without jet flow is almost irrelevant to the surface heat flux. Also, Goldstein et al. [2], Sagot et al. [3], and Paz and Jubran [4] investigated the heat transfer characteristics of jet impingement cooling with respect to the spacing between the jet exit and the impingement plate, besides the jet Reynolds number. Zecchi and Bacci [5] applied a shaped groove to the impinging plate to improve the heat transfer, and found that the embedded groove increases the heat transfer rate in stagnation region and the heat transfer area. Zu et al. [6] conducted a numerical study to examine the effects of the variation of the inclined angle of the jet nozzle on the heat transfer characteristics of an impinging jet cooling system and recommended the SST $k-\omega$ turbulence model for predicting the fluid flow and heat transfer characteristics.

Lee and Lee [7] performed an experimental study on the fluid flow and heat transfer characteristics under a varying jet nozzle-to-plate spacing for an axisymmetric, submerged impinging air jet that was normal to a heated flat plate. And, they presented the correlations in terms of Nusselt number, Reynolds number, and dimensionless nozzle to plate spacing. Chambers et al. [8] analyzed the characteristics of fluid flow under a varying aspect ratio of the elliptic hole. Furthermore, based on a two-dimensional coordinate system, Yang and Tsai [9] presented a numerical simulation of transient conjugate heat transfer in relation to the Reynolds number, orifice to heat-source spacing, and a heated disk condition in the context of the impinging of a high turbulence jet. Lee et al. [10] numerically investigated the characteristics of two-dimensional thermal fluid flow with respect to the Reynolds number and spacing between the jet exit and plate. Kumar and Prasad [11] numerically investigated convective heat transfer with

regard to an effused concave surface with respect to the Reynolds number, jet nozzle-to-surface spacing, exit configuration, and arrangement of holes. Rao et al. [12] experimentally and numerically investigated the heat transfer performance and pressure drop in a multiple jet system (29×29) in a regime of low Reynolds numbers ($<1,000$). Lee and Lee [13] experimentally investigated the heat transfer characteristics of an unconfined elliptic impinging jet for various nozzle aspect ratios. They derived an empirical formula for the stagnation Nusselt number in terms of the aspect ratio and nozzle-to-plate spacing. Lee and Lee [14] confirmed that the shape of the nozzle exit affects heat transfer under impingement and reported that a nozzle with a sharp-edged orifice results in the highest heat transfer rate in the stagnation region from among the tested nozzles, viz., nozzles with sharp-edged, standard-edged, and square-edged orifices, respectively. Using the naphthalene sublimation technique, Oladiran [15] empirically measured the heat transfer coefficient with regard to a target plate with a circular impinging jet in relation to the inclination of the jet nozzle, magnitude of cross flow, and width of the duct. The impinging jet coupled with other internal cooling techniques also has been studied. Funazaki et al. [16–18] investigated the effects of the stand-off distance, pin pitch, and pin array on the heat transfer characteristics of an impinging jet with pin-fin and discharge holes. As for jet impingement on a dimpled plate, Kanokjaruvijit and Martinez-Botas [19] examined the effects of the dimple shape, jet nozzle-to-plate spacing, and position of the impinging jet on the heat transfer rate. Ekkad and Kontrovitz [20] investigated the heat transfer rate depending on the dimple pattern and dimple depth for impingement cooling with dimples on the plate. Rhee et al. [21] performed an experiment to understand the characteristics of fluid flow and heat transfer with regard to an impinging jet with initial cross flow over a ribbed plate with effused holes.

As mentioned above, various investigations have been carried out on the effects of geometric parameters on the heat transfer performance. However, systematic numerical optimization techniques [22] have not yet been applied to the geometries of jet impingement cooling. Among the numerical optimization methods that have been applied with Reynolds-averaged Navier–Stokes (RANS) analyses of fluid flow and heat transfer, the radial basis neural network (RBNN) method [23] has many advantages. The main advantage is the linear nature of RBNN, which reduces the computational cost. Recently, Lee and Kim [24] and Kim et al. [25] applied RBNN to the shape optimization of a film cooling hole and a centrifugal compressor impeller, respectively.

The aims of the present work are to investigate the effects of the jet nozzle shape and the angle of inclination

of the nozzle on the heat transfer characteristics and to optimize the shape of a single impinging jet to improve the heat transfer. Three-dimensional RANS analysis is performed for analyses of fluid flow and heat transfer of the impinging jet. The numerical results are validated with the experimental data, and parametric study with two design variables is performed. And, the RBNN model is employed as an optimization tool to obtain the optimal design.

2 Numerical approach

For a three-dimensional RANS analysis of fluid flow and heat transfer in the context of jet impingement cooling, ANSYS CFX 11.0 [26] is used in this work. The governing differential equations are discretized using the finite volume method. The shear stress transport (SST) turbulence model [27, 28] is used as a turbulence closure. The SST model works by solving a turbulence/frequency-based model ($k-\omega$) at the wall and a $k-\varepsilon$ model in the bulk flow. A blending function ensures a smooth transition between the two models. Bardina et al. [29] showed that the SST model more effectively captures the amount of flow separation under an adverse pressure gradient than other eddy viscosity models, and thus precisely predicts the near-wall turbulence that plays a vital role in the accurate prediction of turbulent heat transfer.

Figure 1 represents the reference configuration considered in the present work. The diameter of the nozzle hole (D) is 12.7 mm and the length of the nozzle is 10D. The length and height of the main channel are 100D and 6D, respectively, and the channel width is 16D. In this simulation, computations are restricted to half the domain to lower the computational time by using the symmetric condition, as shown in Fig. 1. Zu et al. [6] introduced the

validity of the symmetric condition through a comparison between computational results and experimental data.

The computational grid used in this study is represented in Fig. 2 for the entire computational domain and also, near the wall. An unstructured hexahedral grid system is used for the simulation, and the grids are concentrated near the wall and the mixing region to resolve the high velocity gradient. First grid points adjacent to the walls are placed so as to maintain the values of y^+ smaller than 1 to properly implement the low-Reynolds version ($k-\omega$ model) of SST model in near-wall region.

A grid dependency test has been performed on a range of 660,000–3,200,000 nodes to determine the optimum number of grids, as shown in Fig. 3. The plot shows axial distributions of the centerline heat transfer coefficient ratio, h/h_0 , for a blowing ratio of 7.98. Through the test, considering computational economics, the optimal number of grids is determined as being approximately 1,570,000. The mesh of the main channel consists of about 1,552,000 grids, and the jet nozzle part consists of about 21,000 grids.

The heat transfer coefficient is defined as follows:

$$h = \frac{q}{T_w - T_r} \quad (1)$$

where q represents the local heat flux, and T_w and T_r represent the local wall temperature and the reference temperature, respectively. And, adiabatic wall temperature is used as the reference temperature as in most of the previous works [1–3, 5, 7]. The adiabatic wall temperature is defined as the wall temperature at the impingement plate in case without wall heat flux.

The working fluid is the ideal gas (air), and the boundary conditions specified in this simulation are shown in Table 1. At the inlet of the cross flow and jet, a constant mass flow rate is assumed, and the temperature is 298 K.

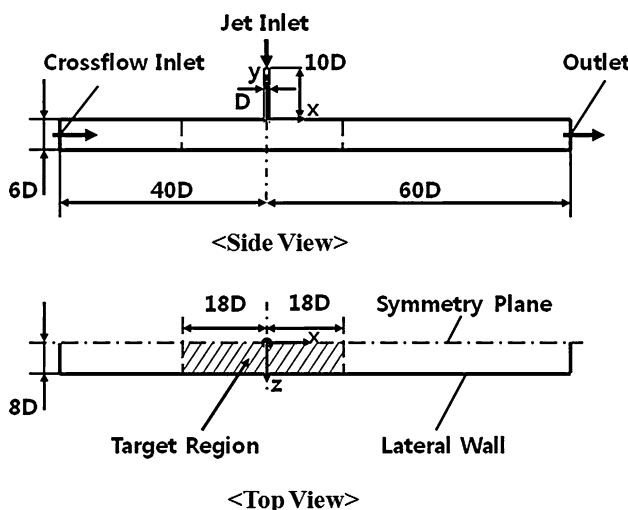


Fig. 1 Schematic of the computational domain

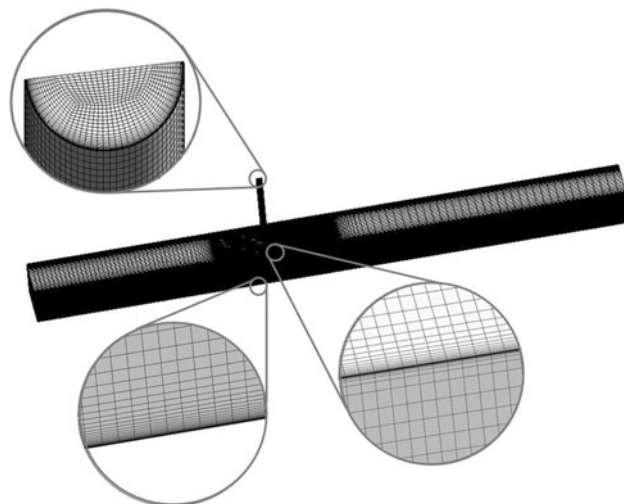


Fig. 2 The computational domain and grid system

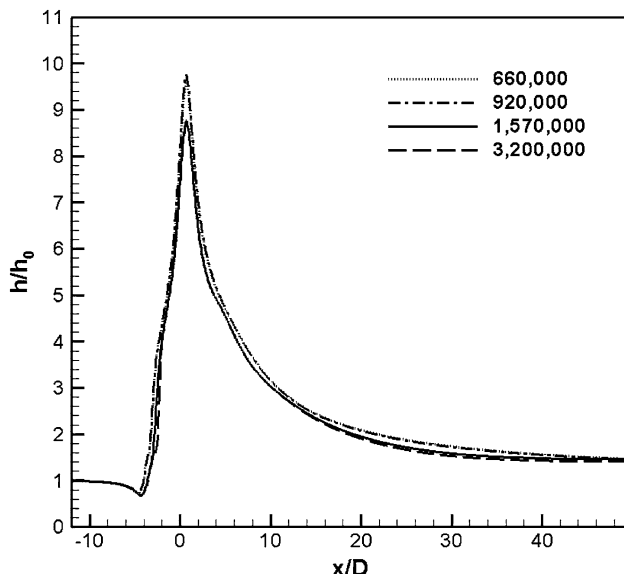


Fig. 3 Grid dependency test

Table 1 Boundary conditions

Boundary	Value
Cross flow Inlet	$U_\infty = 11.96 \pm 0.23[\text{m/s}]$
Jet Inlet	$T = 298[\text{K}]$ $M = 7.98$ $T = 298[\text{K}]$
Impingement Plate	$q = 1200 \text{ W/m}^2$
Rest Wall	No slip and adiabatic
Outlet	1 atm

A uniform heat flux condition is specified for the impingement plate. The blowing ratio (M) is 7.98, and defined as follows:

$$M = \frac{\rho_j U_j}{\rho_\infty U_\infty} \quad (2)$$

where ρ_j and ρ_∞ represent the fluid densities at the exit of the jet nozzle and the main stream, respectively. U_j and U_∞ indicate the average velocities at the exit of the jet nozzle and the main stream, respectively. The no-slip and adiabatic conditions are set at all walls except for the impingement plate.

The present numerical simulations were performed on an Intel Xeon CPU E5420 (a total of eight CPUs). Each calculation was subdivided into eight tasks; data transfer was performed using the MPICH2 [30] local parallel. Parallel computation using eight CPUs helps us to conserve computational time by as much as 35.6% compared to serial computation. The computational time was typically 10–12 h and depended on the geometry considered and the convergence rate. In terms of the convergence criteria, the

limit on the root-mean-square of the relative residual values of all the flow parameters was set to 1.0E-5; the solver finished a single simulation in approximately 1,000 iterations.

3 Design variables and the objective function

Figure 4 shows the geometric variables of a single impinging jet with cross flow. The upper-left figure in Fig. 4 shows a circular hole of the reference jet, while the upper-right figure in Fig. 4 represents an elliptic jet hole shape. The aspect ratio of the elliptic hole (AR) and the angle of inclination of the nozzle (θ) are considered as the design variables. AR is defined as the ratio of the length along the parallel axis (A) to that along the perpendicular axis (B) of the elliptic cross-section, while θ represents the inclination angle in the upstream direction of the cross flow. The area of elliptic hole is maintained as constant as constraint for variation of AR .

The area-averaged Nusselt number for the impingement plane is taken as the objective function. The area-averaged heat transfer coefficient for the target plate is defined as follows:

$$\bar{h} = \frac{\int_{-18}^{18} \int_0^8 h \cdot d(Z/D) \cdot d(X/D)}{36 \times 8} \quad (3)$$

The area-averaged Nusselt number, which is considered as the objective function, is defined as follows:

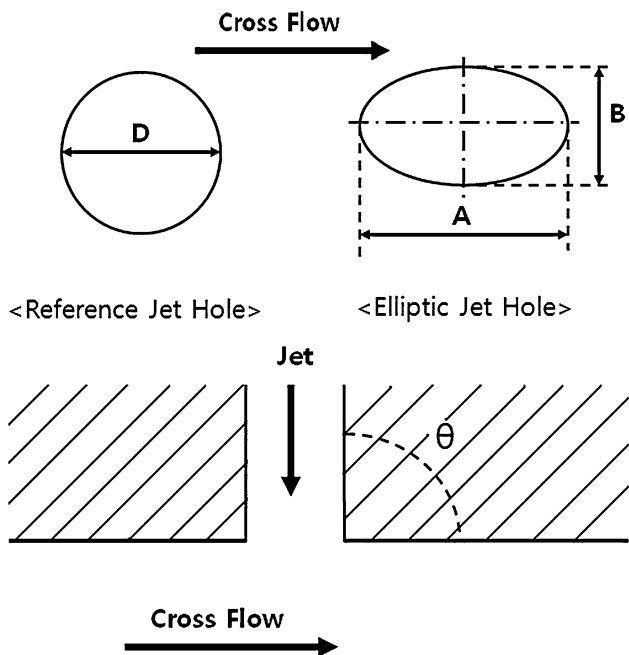


Fig. 4 Schematic of the design variables

$$\overline{Nu} = \frac{\bar{h}D}{\lambda} \quad (4)$$

where λ is the thermal conductivity and D is the jet nozzle diameter (D).

4 Optimization method

Numerical optimization techniques based on surrogate modeling have been effectively used in various engineering applications [22]. In this work, the design optimization of jet impingement cooling with cross flow has been performed using the RBNN model [23]. In the present optimization procedure, two design variables are initially selected and the design space is decided. Then, the twelve design points within the design space are selected using Latin hypercube sampling (LHS) as the design of experiment. The objective function values at these design points are evaluated through the flow solver, and the RBNN model is constructed using the analysis results.

The RBNN model is constructed based on evaluations of the objective function at the prescribed design points through training. The main advantage of using the radial basis approach is the ability to reduce the computational cost due to the linear nature of the radial basis functions. RBNN uses a linear combination of N radially symmetric functions, $\{g_i(x)\}$, for the response function as shown in [23]:

$$F(x_i) = \sum_{i=1}^N w_i g_i(x) + \varepsilon_i \quad (5)$$

where $\{w_i\}$ are the coefficients of the linear combination, $\{g_i\}$ are the radial basis functions, and $\{\varepsilon_i\}$ is the set of errors with equal variance, σ^2 . The RBNN method is a two-layered network with a hidden layer of radial basis transfer functions and linear output. The hidden layer consists of a set of radial basis functions that act as activation functions. The design parameters for this function are a spread constant (SC) and a user-defined error goal (EG). The SC value is selected such that it is not so large that each neuron does not respond in the same manner for all the inputs and it is not so small that the network becomes highly sensitive for every input within the design space.

Error goal (or the mean square error goal selection) is also important. A small error goal will produce over-training of the network, while a large error goal will affect the accuracy of the model. In the present work, we used a customizable RBNN function, *newrb*, which is available in MATLAB [31]. Leave-one-out cross validation (also known as PRESS in polynomial response surface approximation terminology) was performed to assess the accuracy

of the models. Although, it is unclear how well the cross validation correlates with model accuracy, the approach enables nearly unbiased estimation of the generalization errors as it takes into account the cross validation of the surrogate at every design point.

After the RBNN model is constructed, sequential quadratic programming (SQP) (function *fmincon* in MATLAB) has been used as an optimization algorithm. SQP is a robust algorithm for non-linear continuous optimization which is a generalization of Newton's method to multiple dimensions, incorporating a quadratic approximation model for the objective function given an initial guess for the solution. Multiple initial guesses method is used at multiple locations in the design space to avoid local minimum. In this study, best three points among the experimental designs are used as initial guesses. And, the calculations performed in single precision.

5 Results and discussion

In the present work, numerical analysis and optimization of a single impinging jet nozzle with cross flow have been performed using RANS analysis and the RBNN model. First, the numerical results are validated with the experimental data [1]. And, the effects of the two design variables, the aspect ratio of the elliptic hole (*AR*) and the inclination angle of the nozzle (θ), and their coupling effects on heat transfer performance are presented. Finally, the optimization results of impinging jet nozzle shape are demonstrated in last section.

5.1 Validation

First, the present numerical results are validated with the experimental data presented by Bouchez and Goldstein [1]. Fig. 5 shows the axial distributions of the centerline heat transfer coefficient ratio, h/h_0 , for blowing ratios of 7.98 and 10. For $M = 7.98$, the numerical results show generally good agreement with the experimental data except at the stagnation point. In the case of $M = 10$, the present numerical results are compared with the numerical results of Zecchi and Bacci [5] and the experimental data in [1]. Using the k- ϵ turbulence model, Zecchi and Bacci [5] performed numerical simulation for the same geometry as in the present work. As shown in Fig. 5, the present numerical results under the SST turbulence model show better agreement than the previous numerical results [5] in comparison with the experimental data [1]. Sagot et al. [3], Zu et al. [6], and Menter et al. [32] also reported that the SST model produces good results in applications involving impinging jets.

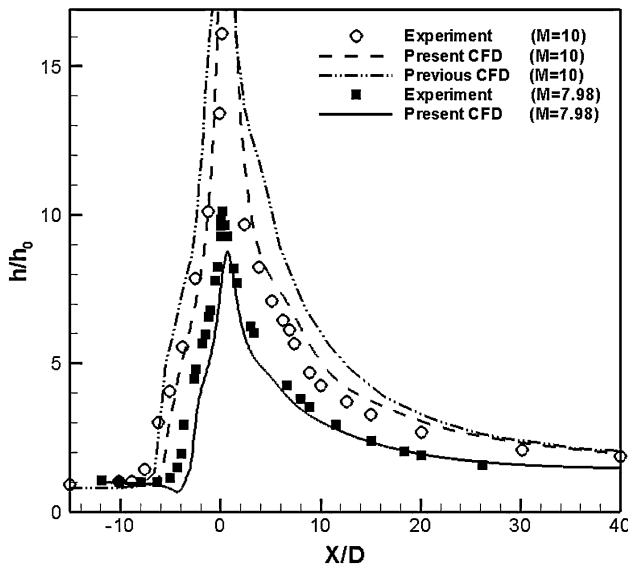


Fig. 5 Validation of the computed results with the experimental data [1]

5.2 The effects of geometric variables

The effects of two geometric variables, viz., the aspect ratio of the elliptic hole (AR) and the inclination angle of the nozzle (θ), on the performance of jet impingement cooling are presented in this section.

Fig. 6 represents variation of the spanwise-averaged Nusselt number distribution along the streamwise direction with AR . The spanwise-averaged Nusselt number is defined as follows:

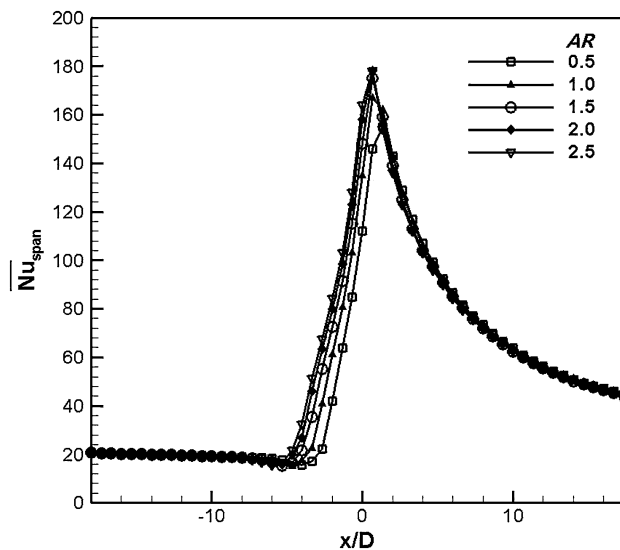


Fig. 6 Distribution of Spanwise averaged Nu along the streamwise direction with AR ($\theta = 90^\circ$)

$$\overline{Nu}_{span} = \frac{\int_0^8 h(x/D, z/D) \cdot d(z/D) \cdot D}{8} \cdot \lambda \quad (6)$$

Spanwise and steamwise mean the directions perpendicular and parallel to the cross flow, respectively. The value at the stagnation point increases with the growth of AR .

Figure 7 shows the variation of the area-averaged Nusselt number with the AR for the reference nozzle angle ($\theta = 90^\circ$). The area-averaged Nusselt number is calculated for the target plate shown Fig. 1. The area-averaged Nusselt number increases with AR in the range of 0.5–2.0.

In Figs. 8 and 9, the flow structure in the channel and heat transfer regarding the target plate are presented with three different ARs of the elliptic jet hole for $M = 7.98$ and $\theta = 90^\circ$. Figure 8 shows the velocity vectors and contours on the symmetric plane in the range of $0.5 < AR < 2.0$. As soon as the flow leaves the nozzle, the jet flow interacts with the cross flow in the main channel; then, diffraction of the jet flow takes place. In the range of testing for AR , the jet flow is diffracted more as AR decreases because a smaller AR leads to a shorter potential core length, as shown in Fig. 8. Figure 8 also shows that the size of the recirculating flow that has taken place just upstream of the impingement becomes smaller as AR decreases. The recirculating flow is generated by the interaction between the wall jet flow induced by the impingement and the cross flow. Therefore, the size of this recirculation is related to the relative strength of the jet impingement. Figure 9 shows the Nusselt number contours for the target plate. The effective heat transfer area due to the jet impingement is reduced and pushed downstream as AR decreases. In the case of $AR = 2.0$, the area of

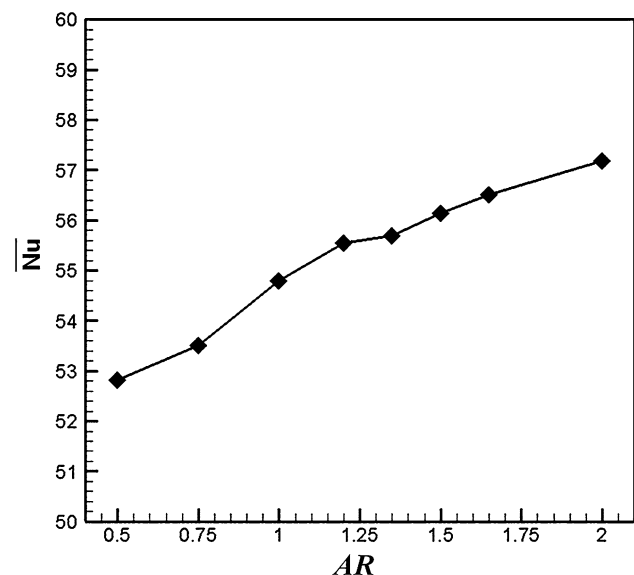


Fig. 7 Variation of the area-averaged Nu with AR ($\theta = 90^\circ$)

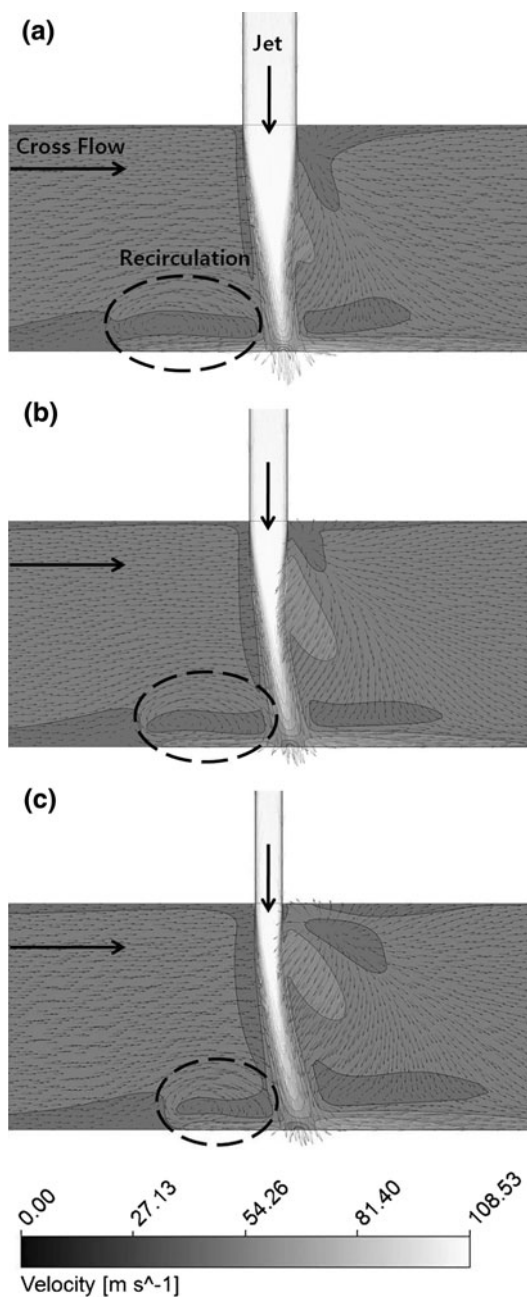


Fig. 8 Velocity vectors and contours on the symmetric ($z = 0$) plane. **a** $AR = 2.0$, **b** $AR = 1.0$, and **c** $AR = 0.5$

high Nusselt number is more widely distributed on the target plate compared to the other cases due to the larger size of the recirculating flow. These results confirm that the bigger AR induces longer potential core length and larger recirculation flow, and these contribute to enhancement of heat transfer rate at stagnation point.

Figure 10 represents distributions of the spanwise-averaged Nusselt number along the streamwise direction with different inclination angles of the jet nozzle ($\theta = 20^\circ$, 45° , 60° , 75° , 90° , and 120°) for $M = 7.98$. This figure

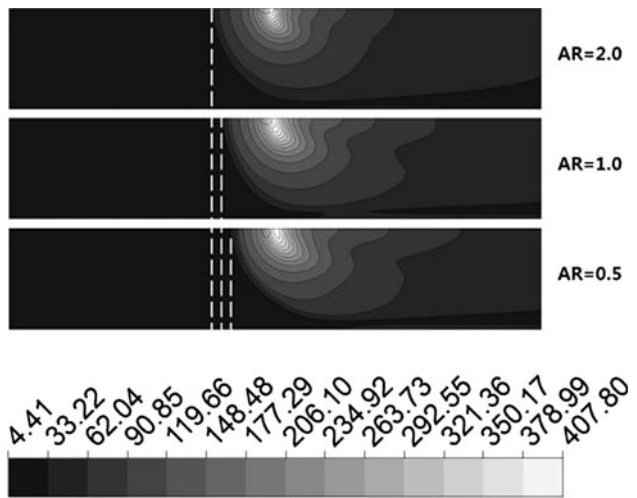


Fig. 9 Nusselt number contours on the target plate

shows that the peak Nusselt number increases with θ when $\theta < 90^\circ$, and the location of the peak Nusselt number moves downstream as the angle increases. This result is the same as that obtained experimentally by Oladiran [15]. He experimentally investigated the effect of the angle of inclination of the jet nozzle (θ) for a single impinging jet with cross flow, and reported that the maximum heat transfer coefficient is obtained at $\theta = 75^\circ$ and 90° , and that the heat transfer coefficient reduces with decreasing θ for a velocity ratio of 8. Figure 11 shows the variation of the area-averaged Nusselt number for a target plate with the angle of inclination of the jet nozzle, viz., θ . The maximum heat transfer performance is observed at $\theta = 45^\circ$. Also, in the range of θ of $75\text{--}90^\circ$, the Nusselt number shows no significant change. Figure 12 represents the velocity vectors and vorticity (ω_z) contours on a symmetric plane for various inclination angles of the jet nozzle (θ). The size of the recirculating flow upstream of the impingement is diminished as θ increases. For $\theta = 20^\circ$, the jet flow does not sufficiently reach the target plate due to bulky mixing between the cross flow and the jet flow; thus, the target plate is not affected enough by the jet flow. This is the reason why the heat transfer rate is lower at this inclination angle, as shown in Fig. 11. On the other hand, in the cases of $\theta = 75^\circ$ and 90° , the Nusselt number at the stagnation point is actually much larger than the others. But, the area-averaged Nusselt number on the target plate for these inclination angles is smaller than that for $\theta = 45^\circ$, as shown in Fig. 11, due to the smaller recirculation region upstream of the impingement, as shown in Fig. 12. Thus, the size of recirculation affects overall heat transfer performance.

As shown above, the optimum Nusselt number for the target plate is found around $\theta = 45^\circ$. Therefore, the effect of AR on the area-averaged Nusselt number is evaluated

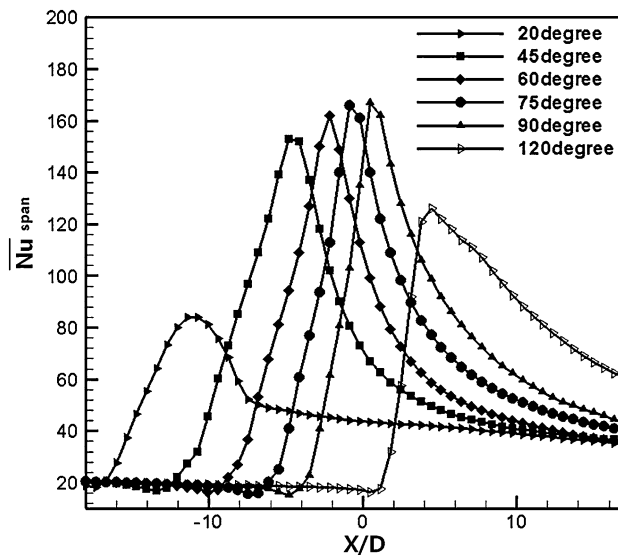


Fig. 10 Distribution of Spanwise averaged \bar{N}_u along the streamwise direction with θ

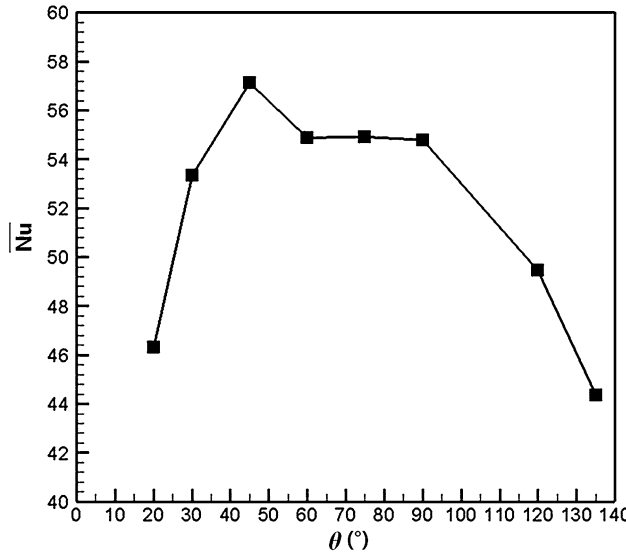


Fig. 11 Variation of the area-averaged \bar{N}_u with θ

again for the jet nozzle inclination angle (θ) of 45° in Fig. 13. In the case of $\theta = 90^\circ$, the Nusselt number increases monotonically with AR as shown in Fig. 9; however, in the case of $\theta = 45^\circ$, the objective function decreases as AR increases beyond the point of maximum heat transfer (at around $AR = 0.9$). A comparison of the flowfields for $AR = 0.5$ and 2.0 ($\theta = 45^\circ$) is shown in Fig. 14. The recirculating flows are formed just upstream and downstream of the jet impingement. The corresponding upstream recirculation regions are similar to each other in shape and size. But, there is an obvious difference with regard to the size of the downstream recirculation region, as shown in Fig. 14. The bigger size of this downstream

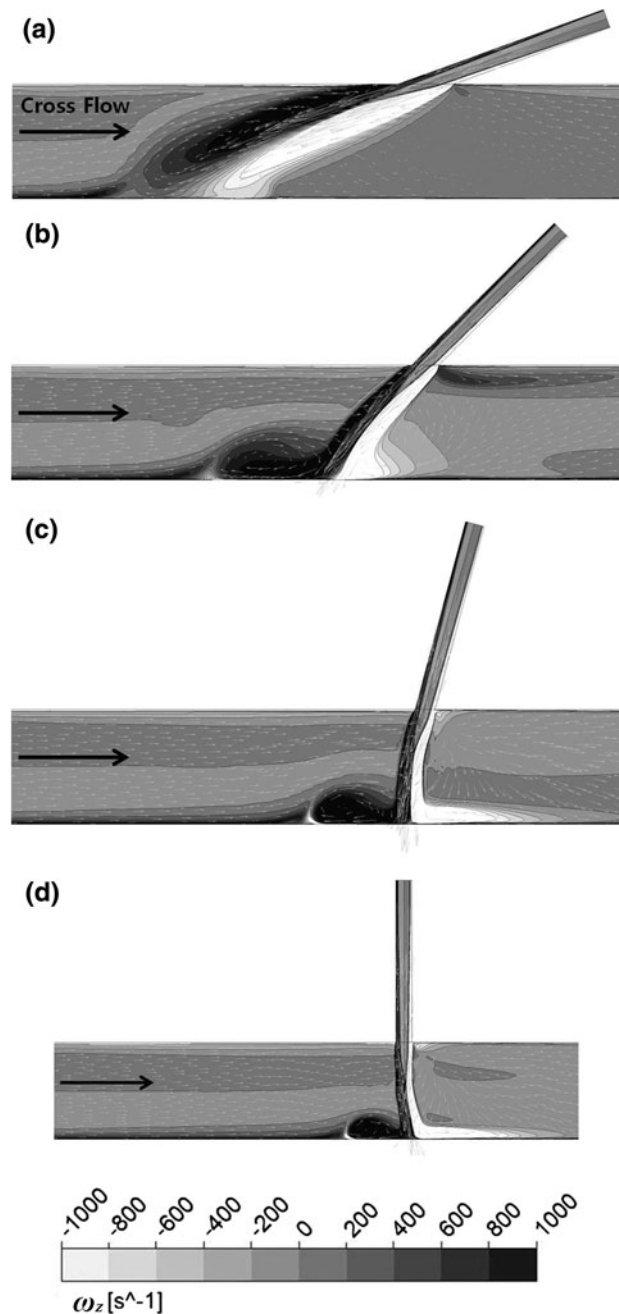


Fig. 12 Velocity vectors and vorticity (ω_z) contours on the symmetric plane: **a** $\theta = 20^\circ$, **b** $\theta = 45^\circ$, **c** $\theta = 75^\circ$, and **d** $\theta = 90^\circ$

recirculation region produces a higher heat transfer rate, as shown in Fig. 13.

5.3 Optimization results

In the present work, for an impinging jet with a blowing ratio of $M = 7.98$, surrogate-based optimization has been performed to enhance heat transfer with two design variables: the inclination angle of the jet nozzle (θ) and the aspect ratio of the elliptic hole (AR). Based on the results of

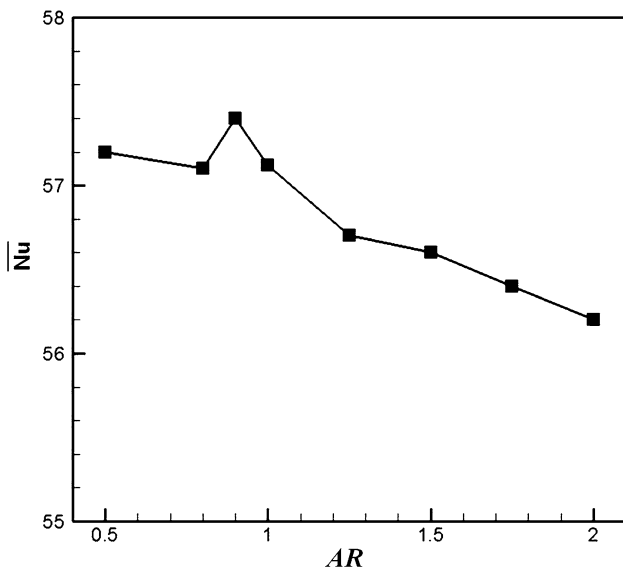


Fig. 13 Variation of the area-averaged Nu with AR ($\theta = 45^\circ$)

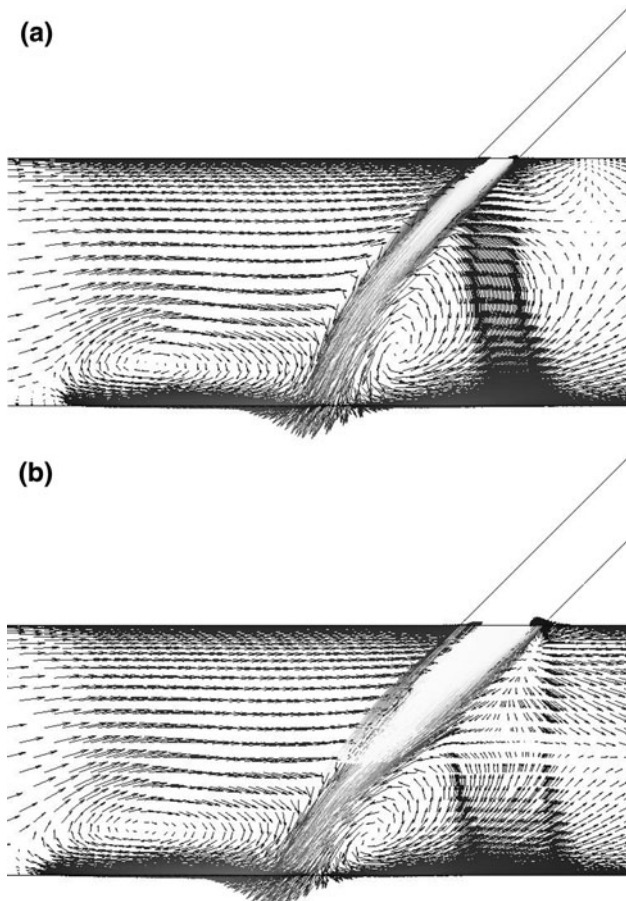


Fig. 14 Velocity vector plots ($\theta = 45^\circ$): **a** $AR = 0.5$ and **b** $AR = 2.0$

In the previous sections, the following ranges of the design variables are determined for optimization: $20 < \theta < 90$ and $0.5 < AR < 1.5$. Twelve experimental points are

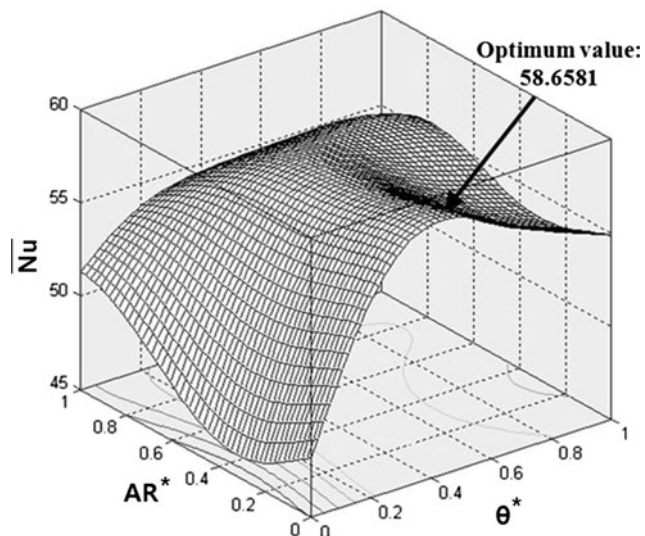


Fig. 15 Three-dimensional plot of the objective function

Table 2 Results of design optimization

Design variable	Objective function			Enhancement	
	θ	AR	RBNN	RANS	
Reference	90.00°	1.000	—	53.86	—
Optimum	50.24°	0.586	58.66	58.11	0.94%

selected by using the Latin hypercube sampling technique, and the objective function, which is defined as the area-averaged Nusselt number on the target plate, is evaluated through RANS analysis at these points. The radial basis neural network (RBNN) model [23] is constructed using the RANS data. Finally, a sequential quadratic programming (SQP) algorithm is used to find the optimal point from the RBNN model.

Figure 15 shows the surface of the RBNN model. The axes (AR^* and θ^*) of the base plane representing the design variables are normalized in the range, $[0, 1]$. The optimal point located at $(0.086, 0.432)$ on the surface is shown in the figure. From this figure, it is evident that the objective function value is more sensitive to θ as compared to AR . Table 2 shows the reference and optimal shapes and their objective function (i.e., the area-averaged Nusselt number) values. The values of θ and AR resulting from optimization are reduced in comparison with the reference shape. The objective function value of the optimized shape obtained by RANS analysis is increased by 7.89% as compared to the reference geometry. Further, the objective function value predicted by RBNN differs from the value calculated by RANS analysis with an error of less than 1%.

Figure 16 shows the distributions of the streamwise-averaged Nusselt number along the spanwise direction for

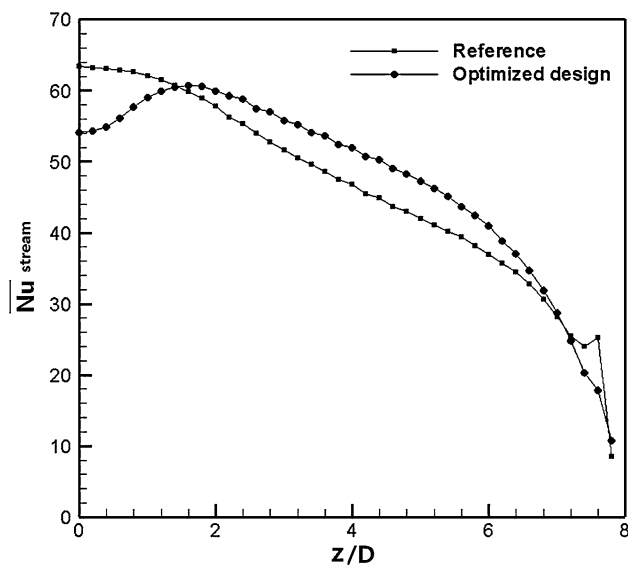


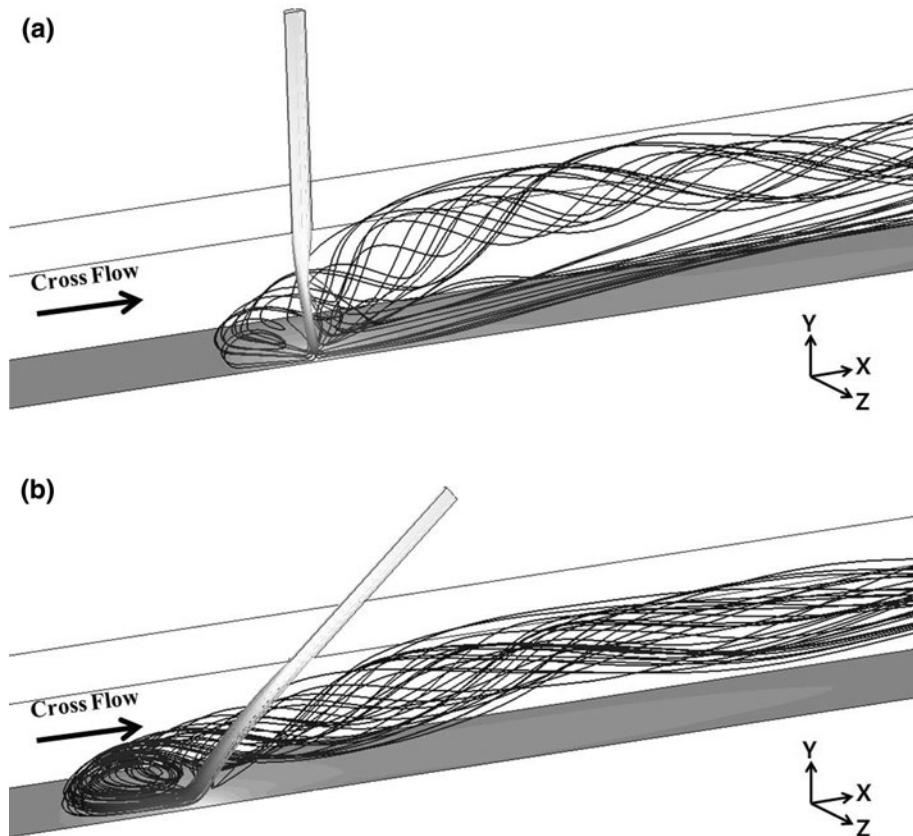
Fig. 16 Comparison between the reference and optimized designs

the optimized and reference shapes. Except when $Z/D < 2$ and in the vicinity of the lateral wall, the heat transfer performance of the optimized shape is better than that of the reference shape as shown in Fig. 16. The streamwise-averaged Nusselt number is defined as follows:

$$\overline{Nu}_{stream} = \frac{\int_{-18}^{18} h(x/D, z/D) \cdot d(x/D)}{36} \cdot \frac{D}{\lambda} \quad (7)$$

The streamlines of the jet flow are presented in Fig. 17. In the reference case, the streamlines issuing from the jet nozzle are split into two groups: one group moves straight downstream with the cross flow after impingement, and the other group moves upstream after impingement to form a recirculating flow. Then, the stream that is heated during the recirculation near the bottom wall moves upward and downstream along the upper wall. On the other hand, most of the streamlines issuing from the optimized jet nozzle move downstream after impingement to join with the recirculating flow and then move together downstream along the upper wall. As mentioned above, the larger upstream recirculation enhances the overall heat transfer with regard to the target wall. Figure 18 represents the distributions of the dimensionless temperature (Φ) on the target plate. The dimensionless temperature is defined as the ratio of the wall temperature to the inlet temperature of the cooling air. The reference shape shows a higher overall temperature distribution on the target plate. In the case of the optimized shape, a wide, low-temperature region spreads over the target plate. The hottest region is found near the lateral wall (dashed lines) in both cases.

Fig. 17 Streamlines of the jet flow: **a** reference shape and **b** optimized shape



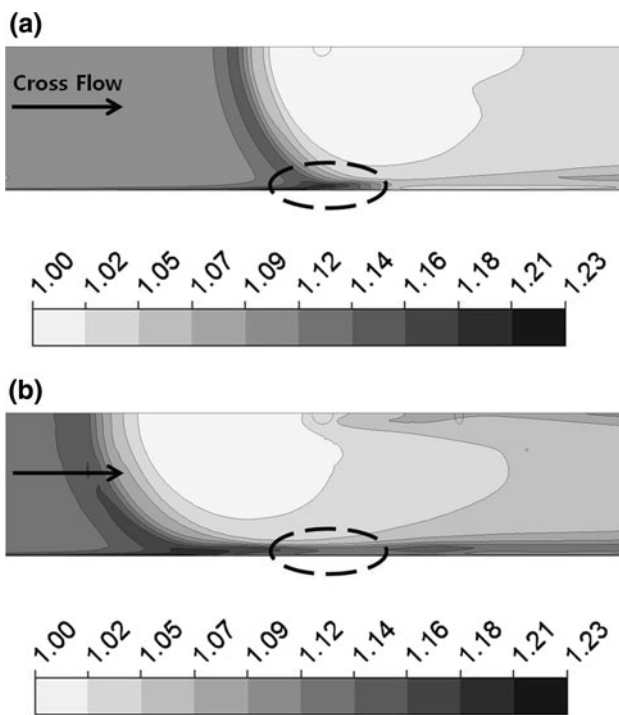


Fig. 18 Dimensionless temperature (Φ) contours on the target plate: **a** reference shape and **b** optimized shape

6 Conclusion

A parametric study and shape optimization of a single jet impingement cooling system with cross flow have been performed to enhance heat transfer performance using three-dimensional RANS analysis. The results of numerical analysis with the SST turbulence model show good agreement with the experimental data. The effects of design variables, specif., the aspect ratio of the elliptic jet nozzle hole and the inclination angle of the jet nozzle, on the heat transfer are evaluated using RANS analysis. It is found that the size of the recirculation region just upstream of the jet impingement and the length of the potential core of the jet are the important flow characteristics that affect the heat transfer on the target plate. Also, the heat transfer is more sensitive to the inclination angle than to the aspect ratio. Twelve design points are selected by the Latin hypercube sampling method within the design space. The aspect ratio and the inclination angle of the optimum shape are found to be 0.586 and 50.24° , respectively, for a blowing ratio of 7.98. Through the optimization using RBNN surrogate modeling, the area-averaged Nusselt number on the target plate is improved by 7.89% as compared to the reference shape. Further, the RBNN accurately predicts the optimum objective function value with a relative error of less than 1% in comparison with that calculated by RANS analysis.

Acknowledgments This work was supported by the National Research Foundation of Korea (NRF) grant No. 2009-0083510 funded by the Korean government (MEST) through Multi-phenomena CFD Engineering Research Center.

References

- Bouchez JP, Goldstein RJ (1975) Impingement cooling from a circular jet in a cross flow. *Int J Heat Mass Transfer* 18:719–730
- Goldstein RJ, Behbahani AI, Heppelmann KK (1986) Streamwise distribution of the recovery factor and the local heat transfer coefficient to an impinging circular air jet. *Int J Heat Mass Transfer* 29(8):1227–1235
- Sagot B, Antonini G, Christgen A, Buron F (2008) Jet impingement heat transfer on a flat plate at a constant wall temperature. *Int J Therm Sci* 47:1610–1619
- Paz MLD, Jubran BA (2008) Predictions of thermal and hydrodynamic characteristics of a single circular micro-jet impinging on a flat plate. In: ASME Turbo Expo 2008, Berlin, Germany, GT2008-50490
- Zecchi S, Bacci A (2004) Numerical analysis of crossflow and single jet impinging on a heated surface with shaped groove. In: ASME Turbo Expo 2004, Vienna, Austria, GT2004-53549
- Zu YQ, Yan YY, Marlson JD (2009) CFD prediction for multi-jet impingement heat transfer. In: ASME Turbo Expo 2009, Orlando, Florida, GT2009-59488
- Lee JH, Lee SJ (1999) Stagnation region heat transfer of a turbulent axisymmetric jet impingement. *Exp Heat Transfer* 12:137–156
- Chambers AC, Gillespie DRH, Ireland PT, Mitchell M (2006) Enhancement of impingement cooling in a high cross flow channel using shaped impingement cooling holes. In: ASME Turbo Expo 2006, Barcelona, GT2006-91229
- Yang YT, Tsai SY (2007) Numerical study of transient conjugate heat transfer of a turbulent impinging jet. *Int J Heat Transfer* 50:799–807
- Lee HG, Yoon HS, Ha MY (2008) A numerical investigation on the fluid flow and heat transfer in the confined impinging slot jet in the low reynolds number region for different channel heights. *Int J Heat Mass Transfer* 51:4055–4068
- Ashok Kumar M, Prasad BVSSS (2009) Computational investigations of flow and heat transfer on an effused concave surface with a single row of impinging jets for different exit configurations. In: ASME Turbo Expo 2009, Orlando, Florida, USA, GT2009-59282
- Arvind Rao G, Kitron Belinkov M, Levy Y (2009) Numerical analysis of a multiple jet impingement system. In: ASME Turbo Expo, Orlando, Florida, USA, GT2009-59719
- Lee JH, Lee SJ (2000) The effect of nozzle aspect ratio on stagnation region heat transfer characteristics of elliptic impinging jet. *Int J Heat Mass Transfer* 43:555–575
- Lee JH, Lee SJ (2000) The effect of nozzle configuration on stagnation region heat transfer enhancement of axisymmetric jet impingement. *Int J Heat Mass Transfer* 43:3497–3509
- Oladiran MT (1981) The effect of nozzle inclination on heat transfer in jet impingement systems. PhD Thesis, Cranfield Institute of Technology
- Funazaki K, Tarukawa Y, Kudo T (2001) Heat transfer characteristics of and integrated cooling configuration for ultra-high temperature turbine blades. In: ASME Turbo Expo, New Orleans, Louisiana, 2001-GT-0148
- Funazaki K, Hachiya K (2003) Systematic numerical studies on heat transfer and aerodynamic characteristics of impingement

- cooling devices combined with pins. In: ASME Turbo Expo 2003, Atlanta, Georgia, USA, GT2003-38256
18. Funazaki K, BinSalleh H (2008) Extensive studies on internal and external heat transfer characteristics of integrated impingement cooling structures for HP Turbines. In: ASME Turbo Expo, Berlin, Germany, GT2008-50202
 19. Kanokjaruvijit K, Martinez-Botas RF (2005) Parametric effects on heat transfer of impingement on dimpled surface. *J Turbomachinery* 127:287–296
 20. Ekkad SV, Kontrovitz D (2002) Jet impingement heat transfer on dimpled target surfaces. *Int J Heat Fluid Flow* 23:22–28
 21. Rhee DH, Nam YW, Cho HH (2004) Local heat/mass transfer with various rib arrangements in impingement/effusion cooling system with crossflow. In: ASME Turbo Expo 2004, Vienna, Austria, GT2004-53686
 22. Samad A, Kim KY (2009) Surrogate based optimization techniques for aerodynamic design of turbomachinery. *Int J Fluid Machinery Systems* 2(2):179–188
 23. Orr MJL (1996) Introduction to radial basis neural network. Center for cognitive science. Edinburgh University, Scotland, UK
 24. Lee KD, Kim KY (2009) Optimization of a fan-shaped hole for film cooling using a surrogate model. In: Proceedings of ASME Turbo Expo, Orlando, Florida, USA, GT2009-59520
 25. Kim JH, Choi JH, Kim KY (2010) Surrogate modeling for optimization of a centrifugal compressor impeller. *Int J Fluid Machinery Systems* 3(1):29–38
 26. Ansys CFX 11.0 (2006) Ansys Inc
 27. Menter F, Esch T (2001) Elements of industrial heat transfer prediction. 16th Bazilian congress of mechanical engineering (COBEM), Uberlandia Brazil
 28. Wilcox DD (1986) Multiscale model for turbulent flows. In: AIAA 24th aerospace science meeting, American Institute of Aeronautics and Astronautics
 29. Bardina JE, Huang PG, Coakley TJ (1997) Turbulence modeling validation. *AIAA J* 35:1997–2121
 30. Thakur R, Groppp W, Toonen B (2005) Optimizing the synchronization operations in message passing interface one-sided communication. *Int J High Perf Comp Appl* 19:11–128
 31. MATLAB®, The language of technical computing, Release 14, The MathWorks Inc, 2004
 32. Menter FR, Kuntz M, Langtry R (2003) Ten year of industrial experience with the SST turbulence model. *Turbulence Heat Mass Transfer* 4:625–632